photonics

MDPI

Article

Regulation of the Second Harmonic Generation of High-Order Poincaré Sphere Beams Using Different Phase Matching

Quanlan Xiao [1], Junsen Yan [1], Xiaohui Ling [2,*] and Shunbin Lu [1,*]

[1] International Collaborative Laboratory of 2D Materials for Optoelectronic Science & Technology of Ministry of Education, Institute of Microscale Optoelectronics (IMO), Shenzhen University, Shenzhen 518060, China; xiaoql@szu.edu.cn (Q.X.); 2300493018@email.szu.edu.cn (J.Y.)
[2] College of Physics and Electronic Engineering, Hengyang Normal University, Hengyang 421002, China
* Correspondence: xhling@hynu.edu.cn (X.L.); shunbin_lu@szu.edu.cn (S.L.)

Abstract

High-order Poincaré sphere (HOPS) beams have attracted tremendous interest due to their complex polarization and phase characteristics. However, manipulating the second harmonics generation (SHG) of HOPS beams is still challenging. Here, we developed a vector-coupled wave model to predict petal-shaped intensity patterns and reveal a linear correlation between petal number and topological order ($n = 2 \rightarrow 4$). Moreover, we experimentally investigated the multidimensional regulation of SHG in HOPS beams through tailored phase-matching strategies. By employing three distinct configurations—(i) type-I phase matching, (ii) type-II phase matching, and (iii) orthogonally arranged BBO crystals based on Type-I phase matching—we establish a comprehensive framework for controlling the spatial and polarization properties of SHG in $n = 2$ HOPS beams. These results advance the manipulation of structured light in nonlinear optics, providing insights for optimizing applications in optical communication and polarization imaging.

Keywords: Poincaré sphere beams; second harmonic generation; phase matching; light field regulation

1. Introduction

High-order Poincaré sphere (HOPS) beams, also known as generalized vector vortex beams, are structured light with complex polarization and phase characteristics [1–4], which have received extensive attention in recent years [5–7]. HOPS beams can be classified into circularly polarized vortex beams, cylindrical vector beams, and elliptically polarized vortex beams [8,9]. The field expression of circularly polarized vortex beams contains a helical phase term $exp(il\varphi)$, indicating that they carry $l\hbar$ of orbital angular momentum, which is of great significance in fields such as quantum information processing [10,11] and orbital angular momentum multiplexing; [12] cylindrical vector beams include radially and azimuthally polarized light, have rotationally symmetric polarization distributions [13,14], and are widely used in laser processing [15], optical trapping [16,17], imaging [18], and so on; elliptically polarized vortex beams allow independent control of spin and orbital angular momentum, which is of great significance in optical communication [19] and manipulation [20].

At present, the processing of vortex light using nonlinear optics has gradually become a hot topic in the field of optical research [21–24], as nonlinear optics can manipulate

Check for updates

Received: 17 February 2026
Revised: 16 March 2026
Accepted: 23 March 2026
Published: 25 March 2026

Copyright: © 2026 by the authors. Licensee MDPI, Basel, Switzerland. This article is an open access article distributed under the terms and conditions of the Creative Commons Attribution (CC BY) license.

the properties of light in multiple aspects such as frequency, polarization, and angular momentum [25–27]. The nonlinear control of vector vortex beams is still in its infancy [28]. How to achieve multidimensional regulation of HOPS through effective and diverse nonlinear means remains an urgent issue to be studied. Taking second harmonic generation (SHG) as an example, by leveraging the polarization selection characteristics of this process and the complex polarization of HOPS, interesting optical field structures can be generated. This paper uses BBO crystal to study the regulation of the SHG of HOPS in terms of polarization characteristics and spatial distribution. BBO has lower cost compared with superstructures [29], and wider thickness selectivity than PPLN [30].

Under different phase-matching conditions, the means of SHG regulation are enriched. Its polarization distribution is controlled by the phase-matching conditions and is manifested as a specific linear polarization state. If two BBO crystals are orthogonally placed for frequency doubling [31], a "petal"-shaped polarization distribution can be obtained, showing complete vector characteristics, and the number of "petals" is positively correlated with the initial order [32,33].

In addition, the frequency-doubling efficiencies of different frequency-doubling methods were measured and discussed. The frequency-doubling efficiency of type-I phase matching is slightly higher than that of type-II phase matching. Moreover, the variation in the frequency-doubling efficiency has certain regularity depending on the initial polarization characteristics.

Hence, three different frequency-doubling processes were carried out using BBO crystals to study the SHG of the Poincaré sphere beam with order n = 2. Based on two types of phase-matching conditions, the vector-coupled wave equations were derived, and the SHGs of circularly polarized vortex beams, cylindrical vector beams, and elliptically polarized vortex beams were simulated accordingly. Finally, the corresponding experimental setup was established to match the simulation results, and the influence of polarization state and frequency-doubling method on the frequency-doubling efficiency was discussed. The experimental results are of great significance for the development of vector nonlinear optics, multi-degree-of-freedom regulation of optical fields, and applications in nonlinear polarization imaging [34] and communication fields [35].

2. Theory

In the process of SHG, two photons of the same frequency interact with each other to generate a photon of a new frequency, which can be described as a steady-state coupled wave equation:

$$\frac{dE^{2\omega}}{dz} = \frac{i\omega d_{eff}}{cn_{2\omega}} E^{\omega} * E^{\omega} e^{i\Delta kz} \tag{1}$$

where $E^{2\omega}$ and E^{ω} represent the SHG and the fundamental frequency (FF) light, respectively; z denotes the transmission distance within the crystal; c, n, and ω are the speed of light, refractive index, and angular frequency, respectively; and d_{eff} is the effective nonlinearity coefficient. In addition, $\Delta k = k_{2\omega} - 2k_{\omega}$ represents the phase mismatch in the SHG process. The phase-matching requirement for the SHG process is that the propagation speeds of the FF and the SHG in BBO should be consistent to minimize destructive interference and maximize the frequency-doubling efficiency.

Quasi-phase matching utilizes the periodic alteration of the polarity of nonlinear crystals to achieve phase matching, while type-I and type-II phase matching rely on the anisotropy of the crystal, but the fabrication process is complex and expensive [36,37]. In the SHG of type-I phase matching (o + o $\rightarrow$ e, for negative uniaxial crystals), that is, when the ordinary light of the fundamental frequency interacts to form the extraordinary light of SHG, only the ordinary light component with the polarization direction

parallel to the crystal's optical axis participates. In the SHG of type-II phase matching (o + e → e, for negative uniaxial crystals), that is, when the ordinary light of the fundamental frequency interacts with the extraordinary light of the fundamental frequency to form the extraordinary light of SHG, two polarization directions are involved. Then, Equation (1) can be rewritten as:

$$\frac{dE_1^{2\omega}}{dz} = \frac{i\omega d_{eff}}{cn_{2\omega}} E_V^{\omega} * E_V^{\omega} e^{i\Delta kz} \tag{2}$$

$$\frac{dE_2^{2\omega}}{dz} = \frac{i\omega d_{eff}}{cn_{2\omega}} E_V^{\omega} * E_H^{\omega} e^{i\Delta kz} \tag{3}$$

$E_1^{2\omega}$ and $E_2^{2\omega}$ represent the horizontal polarization components of the frequency-doubled light obtained from type-I and type-II phase matching, respectively; E_V^{ω} and E_H^{ω} represent the vertical and horizontal polarization components of the fundamental light. Generally, for a HOPS beam with an arbitrary polarization state, it can be expressed as a linear combination of circular polarization bases. The Poincaré sphere beam of the fundamental light can be written in the form of a Jones vector [38]:

$$\begin{aligned} E_{HOPS}^{\omega} &= \left\{ \tfrac{a-b}{2} exp\left[-i(n\varphi + \Phi) \begin{bmatrix} 1 \\ i \end{bmatrix} \right] + \tfrac{a+b}{2} exp\left[-i(n\varphi + \Phi) \begin{bmatrix} 1 \\ -i \end{bmatrix} \right\} * \tilde{E}_0^{\omega} \\ &= \begin{bmatrix} acos(n\varphi + \Phi) + ibsin(n\varphi + \Phi) \\ asin(n\varphi + \Phi) - ibcos(n\varphi + \Phi) \end{bmatrix} * \tilde{E}_0^{\omega} \end{aligned} \tag{4}$$

where a and b represent the major and minor axes of the polarization ellipse, and depend on the polarization state of the light. The ellipticity of the polarization χ has expression $tan\chi = b/a$; for linearly polarized light, $a = 1$, $b = 0$; for circularly polarized light, $a = 1$, $b = 1$; $\exp(in\varphi)$ is the vortex phase of the beam, where n represents the topological charge number and Φ is the polarization direction angle, which is set to 0 in the subsequent experiments. $\tilde{E}_0^{\omega}$ is the intensity distribution function of the initial beam and is a Gaussian beam.

Substituting Equation (4) into Equation (1) and integrating both sides of the equation simultaneously, we can obtain the expressions of SHG obtained in three different ways:

$$E_1^{2\omega} = \frac{i\omega d_{eff}}{cn_{2\omega}} \frac{1}{i\Delta k} [exp(\Delta kL - 1)] \begin{bmatrix} [asin(n\varphi + \Phi) - ibcos(n\varphi + \Phi)]^2 \\ 0 \end{bmatrix} * \tilde{E}_{0V}^{\omega} * \tilde{E}_{0V}^{\omega} \tag{5}$$

$$\begin{aligned} E_2^{2\omega} = \tfrac{i\omega d_{eff}}{cn_{2\omega}} \tfrac{1}{i\Delta k} [exp(\Delta kL - 1)] \{ & \begin{bmatrix} [acos(n\varphi + \Phi) + ibsin(n\varphi + \Phi)]^2 \\ 0 \end{bmatrix} * \tilde{E}_{0H}^{\omega} * \tilde{E}_{0H}^{\omega} \\ & + \begin{bmatrix} [asin(n\varphi + \Phi) - ibcos(n\varphi + \Phi)]^2 \\ 0 \end{bmatrix} * \tilde{E}_{0V}^{\omega} * \tilde{E}_{0V}^{\omega} \} \end{aligned} \tag{6}$$

$$\begin{aligned} E_3^{2\omega} = \tfrac{i\omega d_{eff}}{cn_{2\omega}} \tfrac{1}{i\Delta k} [exp(\Delta kL - 1)] \{ & \begin{bmatrix} 0 \\ [acos(n\varphi + \Phi) + ibsin(n\varphi + \Phi)]^2 \end{bmatrix} * \tilde{E}_{0H}^{\omega} * \tilde{E}_{0H}^{\omega} \\ & + \begin{bmatrix} [asin(n\varphi + \Phi) - ibcos(n\varphi + \Phi)]^2 \\ 0 \end{bmatrix} * \tilde{E}_{0V}^{\omega} * \tilde{E}_{0V}^{\omega} \} \end{aligned} \tag{7}$$

where L is the crystal length, and $E_i^{2\omega}(i = 1, 2, 3)$ represents the SHG obtained by three frequency-doubling methods: (1) type-I phase matching; (2) type-II phase matching; (3) two orthogonally placed BBO crystals with type-I phase matching. Under the condition of small-signal approximation, by using a second-order vortex wave plate to impart

a second-order vortex phase to the fundamental-frequency incident light, the fundamental linearly polarized light, elliptically polarized light, and circularly polarized light will be incident to obtain the corresponding cylindrical vector beam, elliptically polarized vortex beam, and circularly polarized vortex beam, respectively, which are the HOPS beams with $n = 2$. According to Equation (4), when $n = 2$, the expressions corresponding to the three fundamental-frequency polarized lights are as follows:

$$\begin{cases} E^{\omega}_{Cylindrical} = \begin{bmatrix} cos2\varphi \\ sin2\varphi \end{bmatrix} * \tilde{E}^{\omega}_{0} \\ E^{\omega}_{Elliptically} = \begin{bmatrix} (2+\sqrt{2})cos2\varphi + 2isin2\varphi \\ (2+\sqrt{2})sin2\varphi - 2icos2\varphi \end{bmatrix} * \tilde{E}^{\omega}_{0} \\ E^{\omega}_{Circularly} = \begin{bmatrix} cos2\varphi + isin2\varphi \\ sin2\varphi - icos2\varphi \end{bmatrix} * \tilde{E}^{\omega}_{0} \end{cases} \quad (8)$$

The calculation and experimental design of the SHG are carried out according to the above three polarization states, and corresponding simulation and experimental results can be obtained.

3. Results and Discussion

3.1. Experimental Setup

The experimental setup is shown in Figure 1c. A high-power laser (Carbide CB5-06, Light Conversion, Vilnius, Lithuania) with a wavelength of 1030 nm, a repetition rate of 60 kHz, and a pulse width of 225 fs is used as the pump source, with a maximum average power of up to 6 W. To prevent damage to the crystal caused by excessive laser power, a neutral density filter is set up after the laser output as an attenuation system. The light is then polarized by P1, and an arbitrary polarization state is generated by a quarter-wave plate. Subsequently, by adjusting the angle between the optical axis of the vortex plate VP and the polarization direction of the beam, the 0th-order polarized light is transformed into an arbitrary HOPS beam by the vortex plate VP.

Its Jones matrix expression is

$$E_1 = \begin{bmatrix} a\ cos(n\varphi) + b\ sin(n\varphi) \\ a\ sin(n\varphi) - b\ cos(n\varphi) \end{bmatrix} \quad (9)$$

Here, the order n of the VP is 2, which can generate circularly polarized vortex beams, cylindrical vector beams, and elliptically polarized vortex beams with $n = 2$, as shown in Equation (8). The beam waist after VP is measured as ~1 mm. Next, frequency doubling is carried out through a BBO crystal. The BBO crystal is 8 × 8 × 0.8 mm, because the fundamental frequency wavelength is 1030 nm, the phase-matching angle θ of type-I phase matching and type-II phase matching are respectively 23.4° and 33.7°, and d_{eff} are respectively 2.01 pm/V and 1.38 pm/V. The BBO crystals are custom-made, and the light beam is incident perpendicularly onto the BBO crystals for phase matching. Three frequency-doubling methods are adopted here: (1) a single BBO crystal with type-I phase matching; (2) a single BBO crystal with type-II phase matching; (3) two orthogonally placed BBO crystals with type-I phase matching. Since the wavelength of the FF is 1030 nm, the wavelength of the frequency-doubled light is 515 nm. A 600 nm short-pass filter is set to filter out the FF, ensuring accurate observation of the SHG in the CCD.

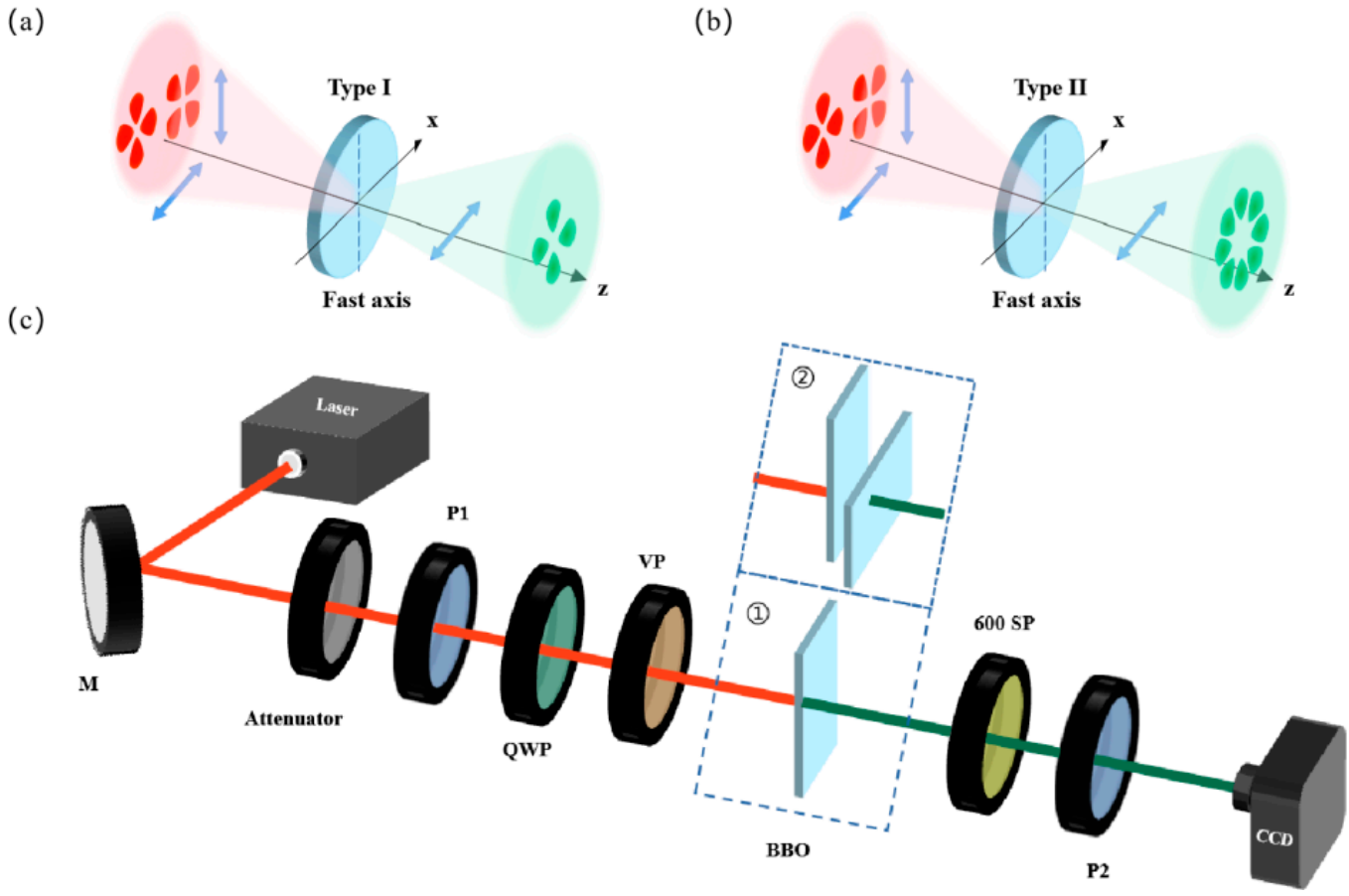


Figure 1. The selection process for spot morphology and polarization state by frequency-doubled light obtained by (**a**) type-I phase matching; (**b**) type-II phase matching; and (**c**) an SHG system using different phase matching. M: mirror; P1, P2: polarizer; QWP: quarter-wave plate; VP: vortex plate; 600 SP: short-pass filter @ 600 nm.

Different spots can be obtained based on different frequency-doubling methods, as shown in Figure 1a,b. The FF passing through the VP is split into horizontal and vertical polarization components. Taking the cylindrical vector beam with $n = 2$ as an example, the morphology of the corresponding polarization components is shown as the black spots in Figure 1. In type-I phase matching, only the vertical polarization component of the FF participates, and the morphology of the SHG spot is inherited from this component, but the polarization changes to horizontal polarization. In type-II phase matching, both the vertical and horizontal polarization components are utilized, and the generated SHG is still a single horizontal linear polarization, but the spot morphology is a composite of the two polarization components of the FF in different directions.

3.2. Theoretical Prediction

From Equations (5) and (6), the expression of the SHG light can be obtained. Then, its Stokes vector is calculated and simulated, as shown in Figure 2b. Figure 2a shows the polarization states in the high-order Poincaré sphere of order $n = 2$. Three polarization states in the figure are selected for study. As can be seen from Figure 2(b1–b3), the fundamental cylindrical vector beam itself has complex polarization characteristics, and its polarization state is marked with black arrows in the figure. The SHG beams obtained by different methods are petal-shaped. The beam obtained by type-I phase matching is 4-petal-shaped, while the beam obtained by type-II phase matching and using orthogonal type-I BBO is 8-petal-shaped. The number of petals is determined by the order n. According to

Equation (9), the Jones matrix expression contains $cos(n\varphi)$ or $sin(n\varphi)$, which becomes $cos(2n\varphi)$ or $sin(2n\varphi)$ after frequency doubling. By calculating the corresponding Stokes vector, it can be known that the intensity of the SHG light obtained by type-I phase matching is proportional to $cos(2n\varphi)$ or $sin(2n\varphi)$, and the intensity of the SHG light obtained by type-II phase matching is proportional to $cos(4n\varphi)$ or $sin(4n\varphi)$. Therefore, the intensity distribution has 4 and 8 peak and valley values, respectively. As can be seen from Figure 2(b3,b6,b9,b12), the SHGs of circularly polarized vortex beams have basically the same spot morphology, all being donut-shaped, with only slight differences in intensity. However, the SHGs of elliptically polarized vortex beams are also petal-shaped, but the peak intensity positions are rotated at a certain angle. Furthermore, the fundamental light and the second harmonic of the cylindrical vector light and the elliptically polarized vortex light are described in Figures S1 and S2 of the Supporting Information. When the order n = 1 or n = 3, the related simulation results are as presented in Figures S3 and S4 of the Supporting Information.

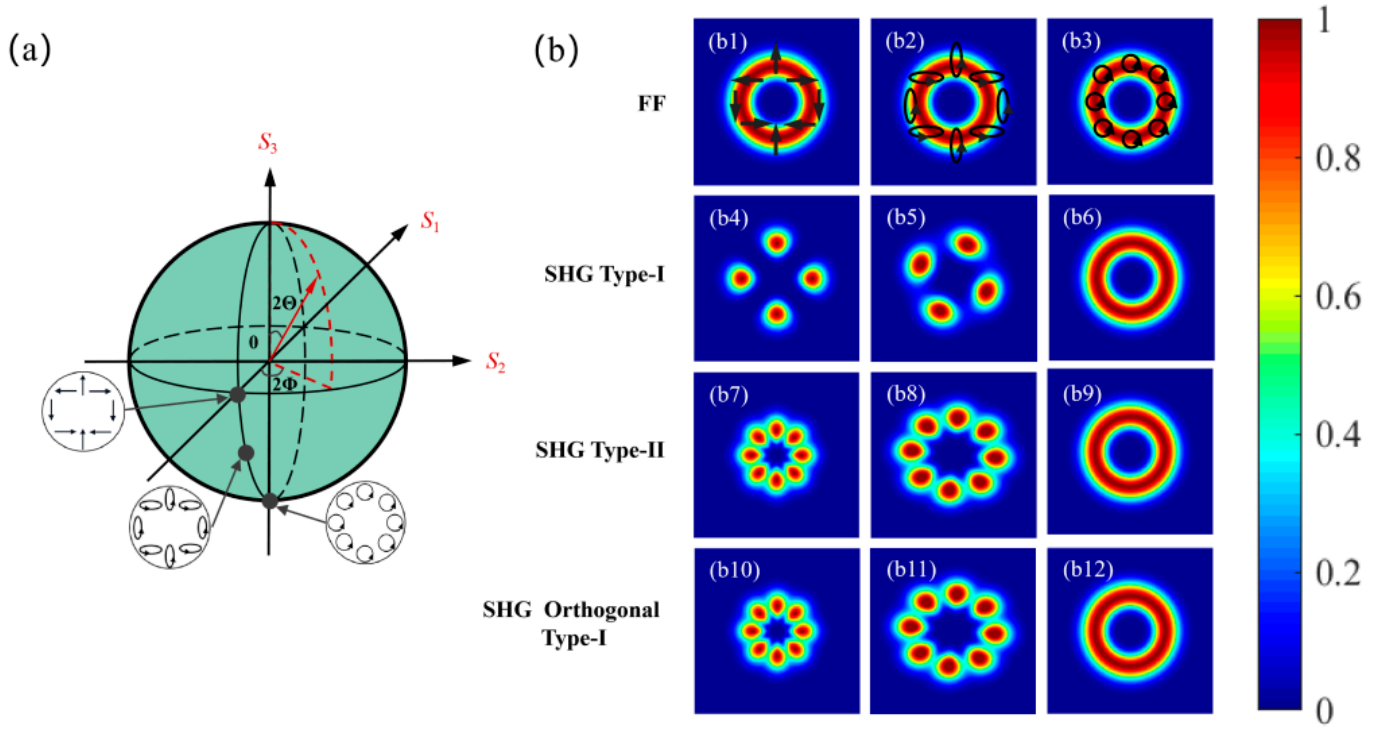


Figure 2. (**a**) HOPS and the polarization state selected for the experiment. The two poles represent circularly polarized vortex light, the points on the equator represent cylindrical vector polarized vortex light, and the points between the two poles and the equator represent elliptically polarized vortex light. (**b**) The theoretical simulation of the intensity and polarization distribution of FF beams and SHG produced by different frequency-doubling methods. (**b1**–**b3**) FF of cylindrical vector light, elliptically polarized vortex light, and circularly polarized vortex light respectively. SHG produced by (**b4**–**b6**) type-I phase matching; (**b7**–**b9**) type-II phase matching; and (**b10**–**b12**) orthogonally placed BBO which is based on type-I phase matching.

3.3. Experimental Results

The frequency-doubling experimental results of the first group of cylindrical vector beams are shown in Figure 3, corresponding to the first column of the simulation results in Figure 2. By rotating the polarizer P2, the corresponding situations of each polarization component of the beam can be observed. Setting the vertical polarization direction in the figure as 0°, the polarization directions from left to right are 45°, 90°, and 135°. It can be found that, when only one BBO is used, the frequency-doubled light has the minimum

intensity in the 0° direction and the maximum intensity in the 90° polarization direction, as shown in Figure 3(b2,b4,c2,c4), indicating that it is a horizontally polarized linearly polarized light. The phase-matching type-I spot morphology has a similarity with the vertical polarization component of the FF, as shown in Figure 3(b1). This comes from the SHG of o + o → e, where only the component in the vertical polarization direction participates; the phase-matching type-II spot morphology is equivalent to the superposition of the vertical polarization component and the horizontal polarization component, as shown in Figure 3(c1). This comes from the SHG of o + e → e, where two polarization components in different directions participate. When using two orthogonally placed BBOs, the frequency-doubled light is no longer a single linearly polarized state but exhibits complex vector characteristics, as shown in Figure 3(d1–d5). When the frequency-doubled light is not polarized by P2, it has an 8-peak intensity distribution, and the polarization spots in the vertical and horizontal directions are 4 peaks. There is a certain angle rotation in the distribution of the light spots, inherited from the horizontal and vertical polarization of the FF respectively; the polarization spot in the 45° direction is similar to the total intensity, only with a difference in intensity, while the polarization spot in the 135° direction is ring-shaped, with a circular dark core in the center. This is due to the efficient utilization of different polarization component directions by the two orthogonally placed BBOs. The SHG of the first BBO utilizes the polarization components parallel to its optical axis, while the other components not participating in this process are utilized by the second BBO, and the final SHG composite results are obtained through the experiment.

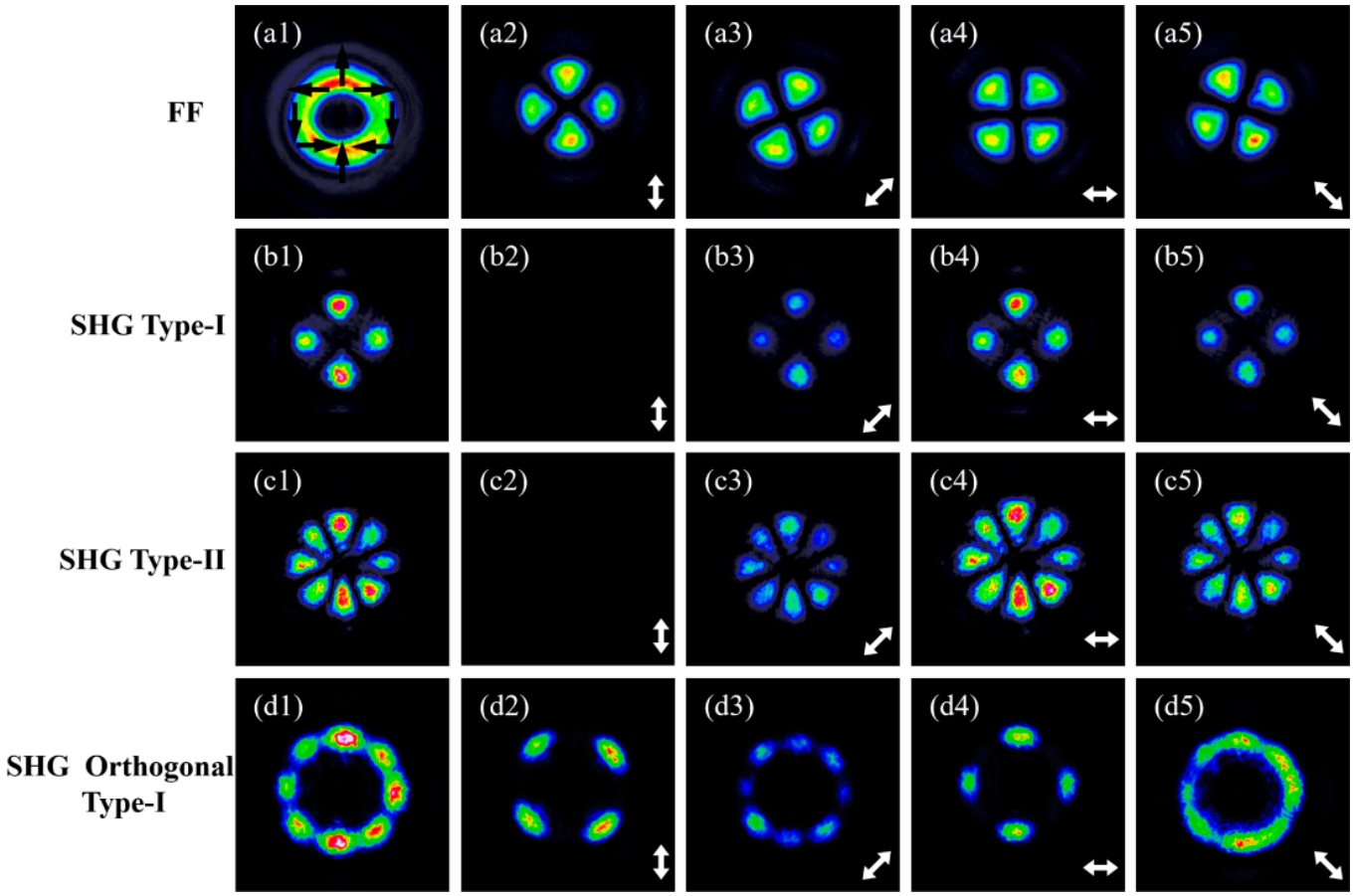


Figure 3. Experimental results of SHG when the FF is a cylindrical vector beam. (**a1**–**a5**) FF and its polarization component at the polarization angles of 0°, 45°, 90°, and 135°. SHG and its polarization component produced by (**b1**–**b5**) type-I phase matching; (**c1**–**c5**) type-II phase matching; and (**d1**–**d5**) orthogonally placed BBO which is based on type-I phase matching.

The frequency-doubling experimental results of the second group of elliptically polarized vortex beams are shown in Figure 4, corresponding to the second column of the simulation results in Figure 2. Similarly, the total light intensity and the polarization components in each direction are given. Due to the change in the FF polarization state, the four-leaf light of the FF continuously connects, and the central dark core becomes square. For the frequency doubling of a BBO, the type-I phase matching gives a four-leaf rotational structure, and the type-II phase matching gives an 8-leaf rotational structure. The light spot is continuous compared to the results of the first group, and the polarization state remains a single linear polarization state. For the frequency doubling of orthogonal BBOs, it still has complex polarization characteristics. Notably, thanks to the change in the FF, its light spot is narrower and longer. Compared with Figure 3(d2,d4), the vertical and horizontal polarization components' distribution in Figure 4(d2–d5) has a certain angle rotation. The morphology of the 45° polarization direction component's light spot is similar to the total light, and the 135° polarization direction component is approximately a circular ring.

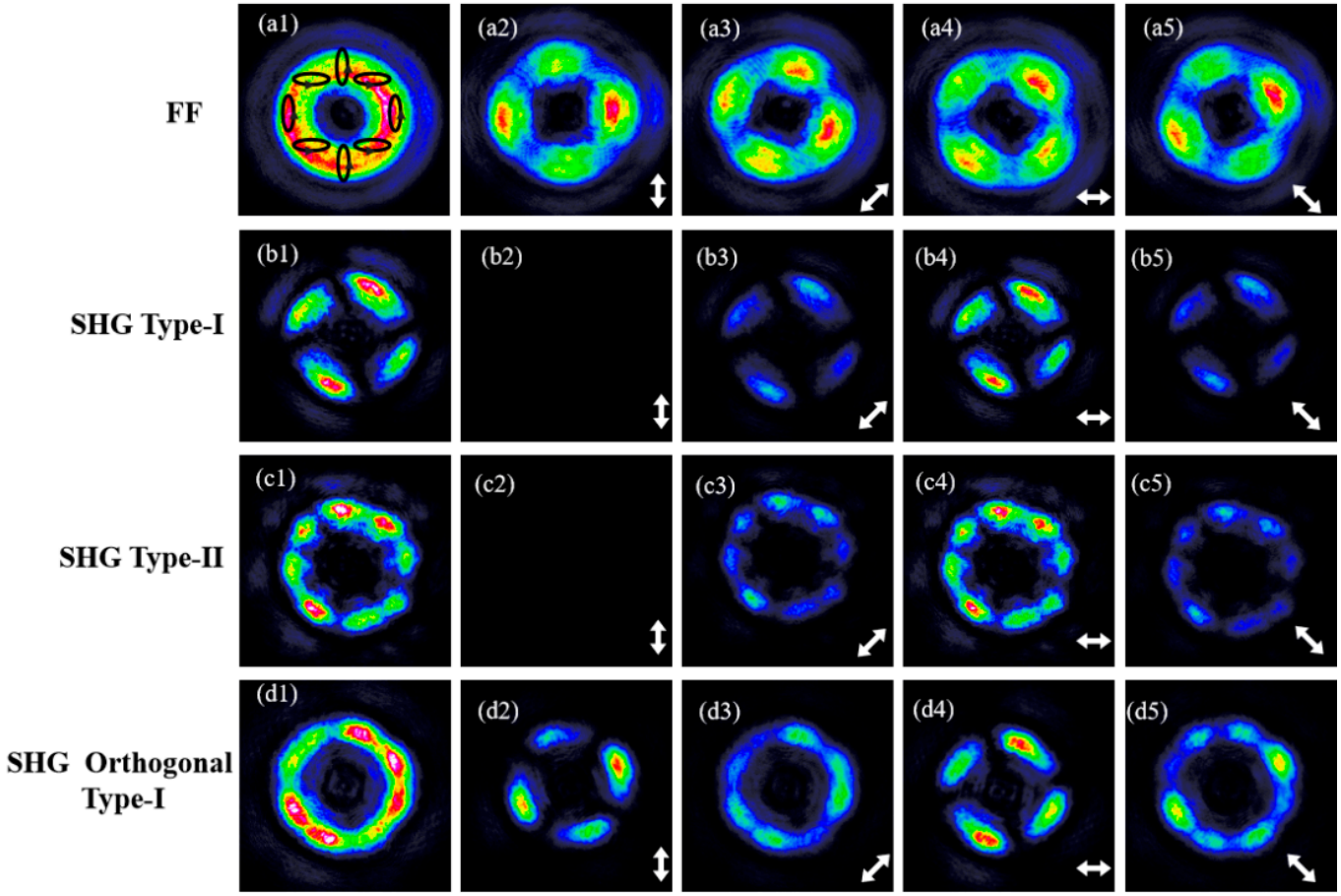


Figure 4. Experimental results of SHG when the FF is an elliptically polarized vortex beam. (**a1**–**a5**) FF and its polarization component at the polarization angles of 0°, 45°, 90°, and 135°. SHG and its polarization component produced by (**b1**–**b5**) type-I phase matching; (**c1**–**c5**) type-II phase matching; and (**d1**–**d5**) orthogonally placed BBO which is based on type-I phase matching.

The experimental results of the SHG of the circularly polarized vortex beam are shown in Figure 5, corresponding to the third column of the simulation results in Figure 2. In fact, the SHG of the circularly polarized vortex beam has almost no change in morphology compared with the FF. Different SHG methods all result in circular ring-shaped light spots with a circular dark core in the center, and the changes before and after are reflected in the topological charge number n representing the orbital angular momentum. After the

light obtained by the second-order VP has a vortex phase exp(i2φ), the topological charge number n of the FF is 2 at this time, and the circularly polarized vortex beam can be imaged by a cylindrical lens for observation, as shown in Figure 5a (right). The resulting image is a linear-shaped light spot with two split lines in the middle, which can be judged as pure second-order vortex light. For the SHG obtained by the three different methods, as shown in Figure 5b–d, it is observed that the splitting number is 4, so the SHG is a fourth-order vortex. This is because, during the process, two photons with the same frequency and the same orbital angular momentum combine to form a new photon. The orbital angular momentum of the initial photon is 2$\hbar$, and the orbital angular momentum of the new photon is the sum of the original photons, which is 4$\hbar$, corresponding to the change in the topological charge number, that is, from n to 2n.

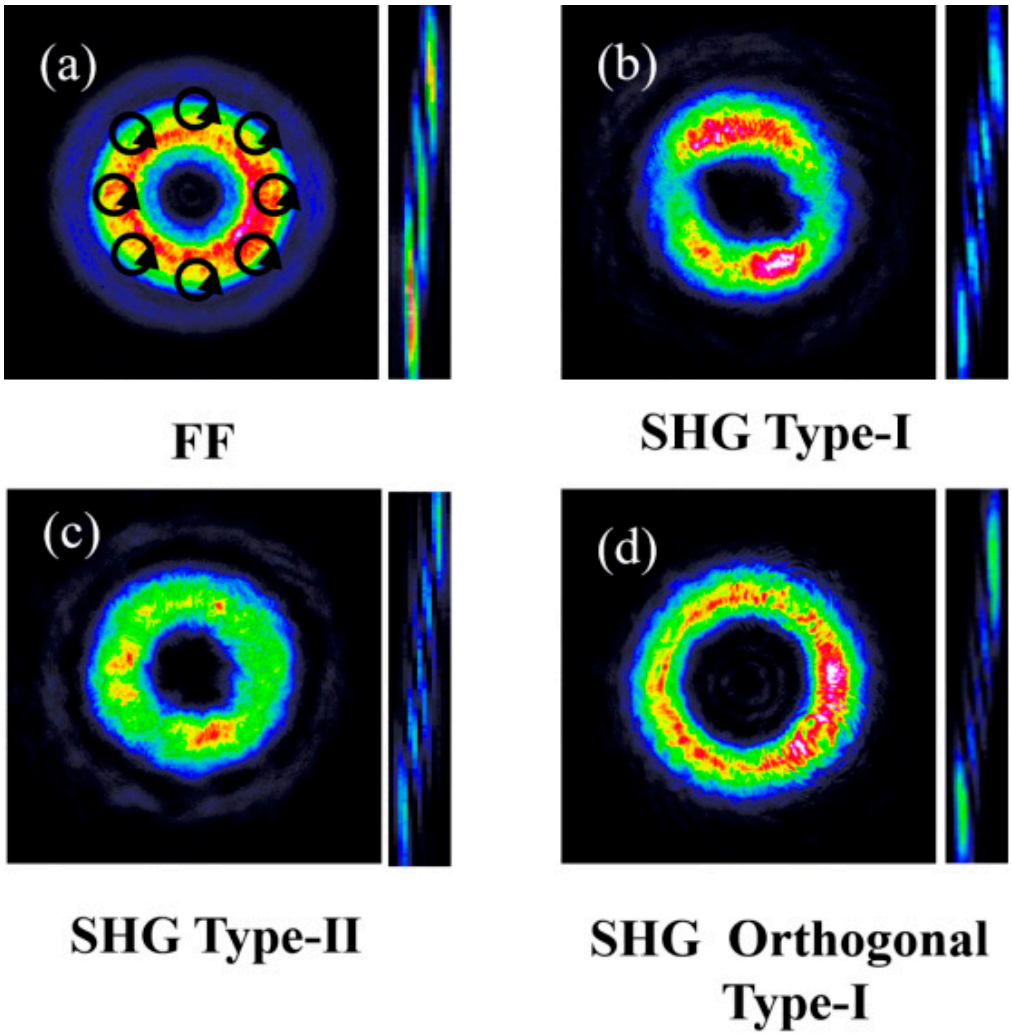


Figure 5. Experimental results of SHG when FF beam is a circularly polarized vortex beam. (**a**) FF and its cylindrical lens imaging. SHG produced by (**b**) type-I phase matching; (**c**) type-II phase matching; and (**d**) orthogonally placed BBO which is based on type-I phase matching. The numbers of black splits in the right of the figures (**a**–**d**) represent the related topological charge n.

Furthermore, by rotating the continuous-wave neutral density filter, changing the power of the FF, and observing the results with a power meter, the influence of different polarization states and different frequency-doubling methods on the frequency-doubling efficiency was studied. As shown in Figure 6a–c, they represent the frequency-doubling efficiency of cylindrical vector light, elliptically polarized vortex light, and circularly po-

larized vortex light, respectively. The power of the FF gradually increased from 100 mW to 400 mW. Figure 6d visually shows the relationship between the frequency-doubling efficiencies under different conditions. Among the three frequency-doubling methods, the frequency-doubling efficiency of type-I phase matching is the highest, followed by type-I phase matching using orthogonal BBO. This is in line with expectations. The efficiency of type-II phase matching is the lowest. This is attributed to the selection of polarization states by the two types of phase matching. Type-I phase matching (o + o → e) participates in the process where the polarization state of the FF is consistent, resulting in higher photon interaction efficiency; type-II phase matching (o + e → e) participates in the process where the polarization state of the FF is perpendicular, resulting in lower photon interaction efficiency. The effective nonlinear coefficient d_{eff} intuitively reflects the photon interaction efficiency. As far as is known, in the frequency-doubling process of the same crystal at the same wavelength, the d_{eff} of type-I phase matching is slightly higher than that of type-II phase matching. As the polarization state of the cylindrical vector light is gradually changed to circularly polarized vortex light, the local polarization state gradually changes from linear to circular. For type-II phase matching and orthogonal placement of BBO frequency-doubling methods, their efficiency gradually increases. This is because, in these two methods, $E^{2\omega} \propto E_H^{\omega} * E_V^{\omega}$, and the product of the two polarization components in the total light intensity gradually increases during the conversion of the polarization state to circular polarization, resulting in an increase in frequency-doubling efficiency. In type-I phase matching, $E^{2\omega} \propto E_V^{\omega} * E_V^{\omega}$; as the conversion process from cylindrical vector light to circularly polarized vortex light takes place, the polarization state participating in the interaction decreases in the total light intensity, resulting in a decrease in frequency-doubling efficiency.

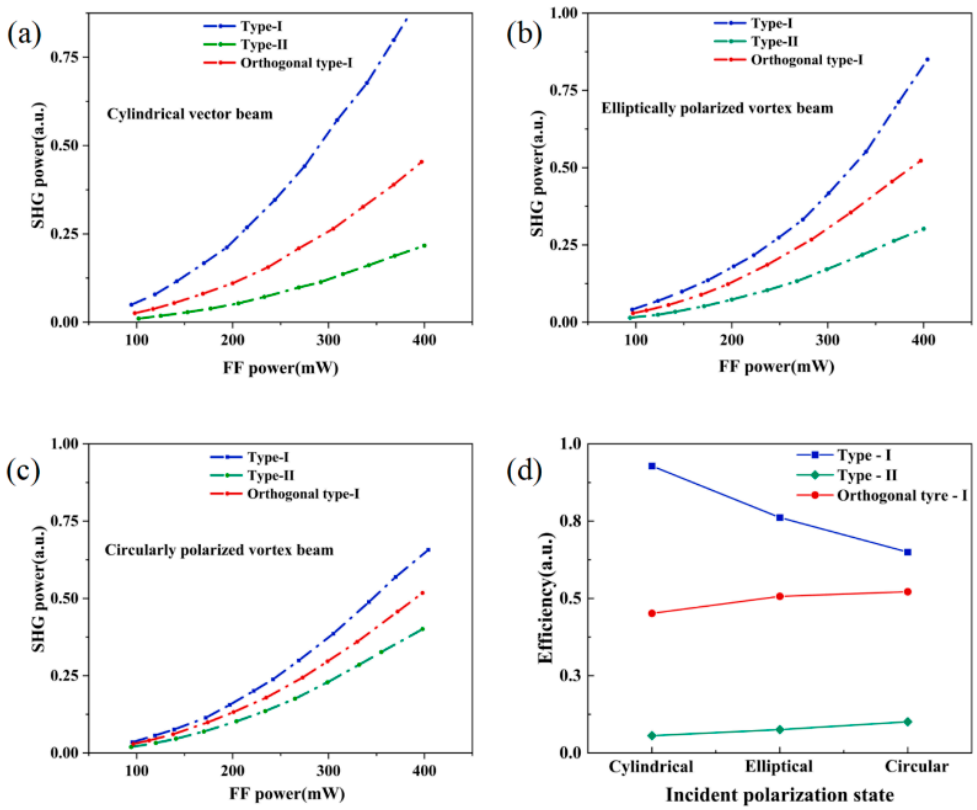


Figure 6. Efficiency of different polarization states or different frequency-doubling modes. SHG power curve of (**a**) cylindrical vector beam; (**b**) elliptically polarized vortex beam; and (**c**) circularly polarized vortex beam. (**d**) Efficiency comparison of different polarization states.

4. Conclusions

In conclusion, the frequency-doubling of HOPS beams was investigated using three different frequency-doubling methods: (1) type-I phase matching, (2) type-II phase matching, and (3) orthogonally placed BBO which is based on type-I phase matching. The vector-coupling wave equation of HOPS beams was derived, and the light spot morphology and polarization state of the frequency-doubled light of the HOPS beams at the $n = 2$ order were verified. In type-I phase matching, it presented a four-lobed structure and was single-line polarized; in type-II phase matching, it presented an eight-lobed structure and was also single-line polarized; in orthogonal placement of BBO, it presented an eight-lobed structure and had complex vector polarization characteristics. It can be known that the number of petals in the light spot structure is proportional to the order n; this is attributed to the $sin(n\varphi)$ and $cos(n\varphi)$ terms in the expression of its Jones matrix. When studying the topological charge number of HOPS beams, in addition to the self-interference system or cylindrical lens imaging methods, the topological charge number of HOPS beams can be inferred from the number of petals of the light spot. Moreover, the topological charge number of circularly polarized vortex beams changes from $n = 2$ to $n = 4$, which is in line with the conservation theorem of angular momentum. This research advances the understanding of using nonlinear effects to control complex polarized beams and provides a new approach for the formation of different patterns of light spots. Among the three frequency-doubling methods, the frequency-doubling efficiency of type-I phase matching is the highest.

Supplementary Materials: The following supporting information can be downloaded at: https://www.mdpi.com/article/10.3390/photonics13040316/s1. Figure S1: Theoretical simulation results of SHG when the FF is a cylindrical vector beam at n = 2; Figure S2: Theoretical simulation results of SHG when the FF is an elliptically polarized vortex beam at n = 2; Figure S3: Theoretical simulation results of SHG when the FF is a cylindrical vector beam at n = 1; Figure S4: Theoretical simulation results of SHG when the FF is a cylindrical vector beam at n = 3.

Author Contributions: Q.X. and J.Y.: Writing—original draft, methodology, conceptualization. S.L.: Writing—review and editing, supervision, resources. X.L.: Writing—review and editing, methodology, supervision, resources. All authors have read and agreed to the published version of the manuscript.

Funding: The authors are grateful for financial support from the Shenzhen Science and Technology Program (JCYJ20220531103016036), Science and Technology Innovation Commission of Shenzhen (20231120235244001), and the Shenzhen Key Laboratory of 2D Meta-materials for Information Technology (ZDSYS201707271014468).

Data Availability Statement: Data are contained within the article.

Conflicts of Interest: The authors declare no conflicts of interest.

References

1. Milione, G.; Sztul, H.I.; Nolan, D.A.; Alfano, R.R. Higher-order Poincaré sphere, Stokes parameters, and the angular momentum of light. *Phys. Rev. Lett.* **2011**, *107*, 053601. [CrossRef]
2. Forbes, A.; De Oliveira, M.; Dennis, M.R. Structured light. *Nat. Photonics* **2021**, *15*, 253–262. [CrossRef]
3. He, C.; Shen, Y.; Forbes, A. Towards higher-dimensional structured light. *Light. Sci. Appl.* **2022**, *11*, 205. [CrossRef]
4. Naidoo, D.; Roux, F.S.; Dudley, A.; Litvin, I.; Piccirillo, B.; Marrucci, L.; Forbes, A. Controlled generation of higher-order Poincaré sphere beams from a laser. *Nat. Photonics* **2016**, *10*, 327–332. [CrossRef]
5. Yao, J.; Jiang, X.; Zhang, J.; Wang, A.; Zhan, Q. Quantitative detection of high-order Poincaré sphere beams and their polarization evolution. *Opt. Express* **2023**, *31*, 3017–3027. [CrossRef]
6. Yao, J.; Jiang, X.; Li, X.; Zhang, J.; Zhan, Q.; Wang, A. Cascaded mode converter for generating high-order Poincaré sphere beams of multiple different orders. *Appl. Phys. Lett.* **2023**, *122*, 181103. [CrossRef]

7. Liang, Y.; Xi, T.; Cao, S.; Liu, L.; Liu, F.; Wan, Z.; Wang, J.; Shao, X. Spatiotemporal vectorial structured light that dynamically varies on higher-order Poincaré sphere. *Opt. Express* **2024**, *32*, 28413–28428. [CrossRef]
8. Hu, Y.; Ma, Z.; Zhao, W.; Zhao, J.; Liu, J.; Jing, Q.; Dou, J.; Li, B. Controlled generation of mode-switchable nanosecond pulsed vector vortex beams from a Q-switched fiber laser. *Opt. Express* **2022**, *30*, 33195–33207. [PubMed]
9. Shen, Y.; Wang, X.; Xie, Z.; Min, C.; Fu, X.; Liu, Q.; Gong, M.; Yuan, X. Optical vortices 30 years on: OAM manipulation from topological charge to multiple singularities. *Light. Sci. Appl.* **2019**, *8*, 90. [CrossRef] [PubMed]
10. Cicek, K.; Hu, Z.; Zhu, J.; Meriggi, L.; Li, S.; Nong, Z.; Gao, S.; Zhang, N.; Wang, X.; Cai, X.; et al. Integrated optical vortex beam receivers. *Opt. Express* **2016**, *24*, 28529–28539. [CrossRef]
11. Zhu, Y.; Lu, B.; Fan, Z.; Yue, F.; Zang, X.; Balakin, A.V.; Shkurinov, A.P.; Zhu, Y.; Zhuang, S. Geometric metasurface for polarization synthesis and multidimensional multiplexing of terahertz converged vortices. *Photonics Res.* **2022**, *10*, 1517–1532. [CrossRef]
12. Wang, J. Advances in communications using optical vortices. *Photonics Res.* **2016**, *4*, B14–B28. [CrossRef]
13. Cao, L.; Zhang, M.; Dou, J.; Zhao, J.; Hu, Y.; Li, B. Controlled generation of order-switchable cylindrical vector beams from a Nd: YAG laser. *Chin. Opt. Lett.* **2023**, *21*, 101401. [CrossRef]
14. Chen, S.; Li, J.; Ueda, K. Generation of nanosecond pulsed azimuthally and radially polarized beams with an actively Q-switched rotating disk laser. *Appl. Phys. Lett.* **2021**, *119*, 091103. [CrossRef]
15. Xu, C.; Hu, H.; Liu, Y.; Deng, D. Radially polarized symmetric Airy beam. *Opt. Lett.* **2020**, *45*, 1451–1454. [CrossRef] [PubMed]
16. Zhan, Q. Trapping metallic Rayleigh particles with radial polarization. *Opt. Express* **2004**, *12*, 3377–3382. [CrossRef] [PubMed]
17. Kozawa, Y.; Sato, S. Optical trapping of micrometer-sized dielectric particles by cylindrical vector beams. *Opt. Express* **2010**, *18*, 10828–10833. [CrossRef] [PubMed]
18. Kozawa, Y.; Matsunaga, D.; Sato, S. Superresolution imaging via superoscillation focusing of a radially polarized beam. *Optica* **2018**, *5*, 86–92. [CrossRef]
19. Wang, J.; Yang, J.Y.; Fazal, I.M.; Ahmed, N.; Yan, Y.; Huang, H.; Ren, Y.; Yue, Y.; Dolinar, S.; Tur, M.; et al. Terabit free-space data transmission employing orbital angular momentum multiplexing. *Nat. Photonics* **2012**, *6*, 488–496. [CrossRef]
20. Zhan, Q. Cylindrical vector beams: From mathematical concepts to applications. *Adv. Opt. Photonics* **2009**, *1*, 1–57. [CrossRef]
21. Buono, W.T.; Forbes, A. Nonlinear optics with structured light. *Opto-Electron. Adv.* **2022**, *5*, 210174. [CrossRef]
22. Zhu, Y.; Wang, H.; Zhang, Y.; Liu, D.; Zhong, W.; Gao, Z.; Cui, G.; Lu, Y.; Zhang, Y.; Xiao, M. Generation of an ultra-long sub-diffracted second-harmonic optical needle from a periodically poled LiNbO3 crystal. *Appl. Phys. Lett.* **2020**, *116*, 081106. [CrossRef]
23. Coudrat, L.; Boulliard, G.; Gérard, J.M.; Lemaître, A.; Degiron, A.; Leo, G. Unravelling the nonlinear generation of designer vortices with dielectric metasurfaces. *Light. Sci. Appl.* **2025**, *14*, 51. [CrossRef] [PubMed]
24. Pan, C.; Li, H.; Pang, H.; Ru, R.; Zhang, S.; Wei, D.; Chen, H.; Gao, H.; Li, F. Generation and Manipulation of Spin-Orbit Coupling mode via Four-Wave Mixing with Quantum Interference. *Laser Photonics Rev.* **2024**, *18*, 2300625.
25. Franken, E.P.; Hill, A.E.; Peters, C.W.; Weinreich, G. Generation of optical harmonics. *Phys. Rev. Lett.* **1961**, *7*, 118. [CrossRef]
26. Maker, P.D.; Terhune, R.W. Study of optical effects due to an induced polarization third order in the electric field strength. *Phys. Rev.* **1965**, *137*, A801–A818. [CrossRef]
27. Molina-Terriza, G.; Torres, J.P.; Torner, L. Twisted photons. *Nat. Phys.* **2007**, *3*, 305–310. [CrossRef]
28. Wu, H.J.; Yang, H.R.; Rosales-Guzmán, C.; Gao, W.; Shi, B.S.; Zhu, Z.H. Vectorial nonlinear optics: Type-II second-harmonic generation driven by spin-orbit-coupled fields. *Phys. Rev. A* **2019**, *100*, 053840. [CrossRef]
29. Chen, S.; Li, K.; Deng, J.; Li, G.; Zhang, S. High-order nonlinear spin–orbit interaction on plasmonic metasurfaces. *Nano Lett.* **2020**, *20*, 8549–8555. [CrossRef]
30. Jiang, Q.; Zhao, M.; Wang, Y.; Wang, S.; Dou, J.; Liu, J.; Li, B.; Hu, Y. Second harmonic of higher-order Poincaré sphere beam with two orthogonal 5% MgO: PPLN crystals. *APL Photonics* **2024**, *9*, 056111. [CrossRef]
31. Kwiat, P.G.; Waks, E.; White, A.G.; Appelbaum, I.; Eberhard, P.H. Ultrabright source of polarization-entangled photons. *Phys. Rev. A* **1999**, *60*, R773. [CrossRef]
32. Marrucci, L.; Manzo, C.; Paparo, D. Optical spin-to-orbital angular momentum conversion in inhomogeneous anisotropic media. *Phys. Rev. Lett.* **2006**, *96*, 163905. [CrossRef]
33. Tang, Y.; Li, K.; Zhang, X.; Deng, J.; Li, G.; Brasselet, E. Harmonic spin–orbit angular momentum cascade in nonlinear optical crystals. *Nat. Photonics* **2020**, *14*, 658–662. [CrossRef]
34. Zhu, Z.; Zhang, D.; Xie, F.; Ma, J.; Chen, J.; Gong, S.; Wu, W.; Cai, W.; Zhang, X.; Zhang, X.; et al. Nonlinear polarization imaging by parametric upconversion. *Optica* **2022**, *9*, 1297–1302. [CrossRef]
35. Sit, A.; Bouchard, F.; Fickler, R.; Gagnon-Bischoff, J.; Larocque, H.; Heshami, K.; Elser, D.; Peuntinger, C.; Günthner, K.; Heim, B.; et al. High-dimensional intracity quantum cryptography with structured photons. *Optica* **2017**, *4*, 1006–1010. [CrossRef]
36. Armstrong, J.A.; Bloembergen, N.; Ducuing, J.; Pershan, P.S. Interactions between light waves in a nonlinear dielectric. *Phys. Rev.* **1962**, *127*, 1918.

37. Fejer, M.M.; Magel, G.A.; Jundt, D.H.; Byer, R.L. Quasi-phase-matched second harmonic generation: Tuning and tolerances. *IEEE J. Quantum Electron.* **1992**, *28*, 2631–2654. [CrossRef]
38. Ma, Z.; Zhao, W.; Zhao, J.; Liu, J.; Jing, Q.; Dou, J.; Li, B.; Hu, Y. Generation of arbitrary higher-order Poincaré sphere beam from a ring fiber laser with cascaded Q-plates. *Opt. Laser Technol.* **2022**, *156*, 108552. [CrossRef]

Disclaimer/Publisher's Note: The statements, opinions and data contained in all publications are solely those of the individual author(s) and contributor(s) and not of MDPI and/or the editor(s). MDPI and/or the editor(s) disclaim responsibility for any injury to people or property resulting from any ideas, methods, instructions or products referred to in the content.